TELKOMNIKA Telecommunication, Computing, Electronics and Control
Vol. 99, No. 1, February 2099, pp. 1∼1x
ISSN: 1693-6930, DOI: 10.12928/TELKOMNIKA.v99i1.paperID

System Identification and Cascade PID Controller Design of a Spinbath Circulation Process

Immanuel Raynaldo Santjoko, Tua Agustinus Tamba, Ali Sadiyoko
Center for Control, Automation, and Systems Engineering, Department of Electrical Engineering, Faculty of Engineering Technology
Parahyangan Catholic University, Bandung 40141, Indonesia

Article Info

Article history:

Received mm dd, yyyy
Revised mm dd, yyyy
Accepted mm dd, yyyy

Keywords:

Fluid Dynamics
System Identification
Cascade PID
Automation
Process Control

ABSTRACT

This paper develops a framework for model identification and control system design to enhance the robustness of a spinbath circulation process. The dynamic model of the spinbath process is developed using a grey box modeling approach based on historical data of the steady-state operation of the process. In particular, the analytical parts of the model is first derived using concepts from fluid mechanics which are linearized at equilibrium points to obtain a linear second-order transfer function model with time delay. The model parameters are then estimated on the basis of historical data using curve fitting and nonlinear optimization methods. Using the obtained dynamic model, three types of control system configurations are then constructed, namely single-loop controller, conventional cascade controller, and summed-setpoint cascade controller. The performance of the obtained dynamic model and closed loop control systems are evaluated using numerical simulations. For the modeling part, the validation of the developed model with respect to the historical data showed a fitting value of 86.7382%. With regard to the constructed control systems, it was found that the summed-setpoint cascade control configuration maintains the spinbath solution height in the head tank better than those of the single-loop and cascade control configurations, achieving a 61.29% smaller peak error and 67.84% smaller IAE.

This is an open access article under the CC BY-SA license.

Corresponding Author:

Tua A. Tamba
Department of Electrical Engineering, Parahyangan Catholic University
Bandung, Indonesia
Email: ttamba@unpar.ac.id

1. INTRODUCTION

Viscose Staple Fiber (VSF) is a fiber made from wood pulp, which is chemically processed to produce a fiber that resembles cotton and can be used in textile industries. In the VSF manufacturing process, a viscose solution is sprayed through a spineret into a spinbath solution on a spinning machine [1, 2]. This process causes cellulose in the viscose solution to coagulate into filaments, and accompanied by the release of chemical compounds such as water, H_2S, and CS_2 [3]. Over time, the spin bath solution undergoes dilution and contamination processes, which consequently require filtration and evaporation processes to take place in the next process sequence[1]. Recovery of the spinbath solution occurs in the spinbath circulation system through several steps as illustrated in Figure 1. The spinbath solution is first pumped from the bottom tank to the filter, which is then directed partially to the evaporator and partially to the head tank. Next, the head tank supplies the spinbath solution to the spinning machine with the help of gravitational force such that the flow rate is influenced by the level of the liquid in the head tank and the difference on elevation between the spinning machine

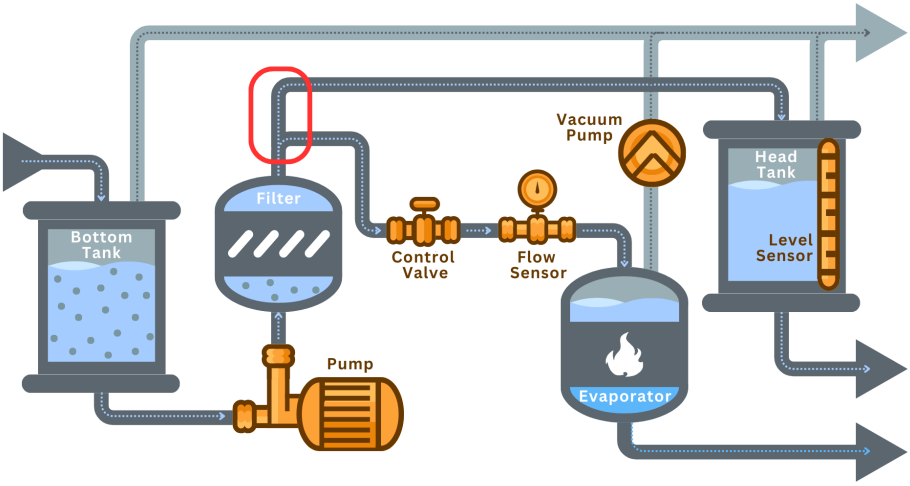

Figure 1. Schematic of spinbath circulation system.

and the head tank. During this process, the level of liquid in the head tank must be kept constant to ensure the production of high quality VSF. Such an absence or reduction of deviations in the liquid level in the head tank during changes in the evaporator inflow setpoint provides various benefits. First, it simplifies the operatorss work on handling decentralized control system (DCS) by automating the process of shutdown and activating the evaporator. Second, it improves overall system reliability, reducing the risk of human error and unwanted downtime. Third, it enhances VSF quality due to consistent spinbath solution flow rates. Finally, it has the potential to reduce operational costs and increase company profits.

In the spinbath circulation system, it is important to note that the channels of the spinbath solution from the filter to the head tank and to the evaporator are interconnected. As a result, any change in the inflow rate of the evaporator that is controlled by a control valve will affect the inflow rate to the head tank, and gradually may impact the level of the liquid in the head tank. In particular, based on the field observation of a real spinbath process considered in this paper, the speed of the pump which supplies the inflow rate to the evaporator is manipulated based only on the level of the liquid in the head tank. In other words, changes in the evaporator inflow setpoint are currently not compensated for by the existing control system in the head tank. Consequently, the process of shutting down and activating the evaporator process can cause significant deviations of the liquid level in the head tank if it is not done carefully and in a gradual manner.

To address the present limitation of the considered spinbath process, this research proposed a more systematic procedures for the modeling and control systems design steps of the process. In the proposed procedure, each component of the spinbath process is first modeled analytically using concepts from static fluid mechanics to describe the relationship between input and output signal of the component [4, 5]. Subsequently, each model is linearized and represented as a second-order linear system transfer function with a time delay [6]. The parameters of the obtained analytical models are then estimated on the basis of historical data using curve fitting and nonlinear optimization techniques [7]. Using the validated dynamic model, three types of control system configurations are then constructed, namely single-loop controller, conventional cascade controller, and summed-setpoint cascade controller [8, 9]. The performance of the obtained dynamic model and closed-loop control systems are finally evaluated and compared using numerical simulations.

2. DYNAMIC MODELING METHOD

As illustrated in Figure 2, the dynamic modeling of the spinbath circulation process begins with the derivation of the static model of each process component under steady state operating condition, and then continues with model linearization to obtain a linear transfer function with time delay compensation for each of such components. The system schematic in Figure 2 shows several inspection points where process variables/parameters can be observed and used in the static modeling process, such as pressure (p), velocity (v), flow rate (Q), and elevation (z). The system consists of several major elements and variables, namely the

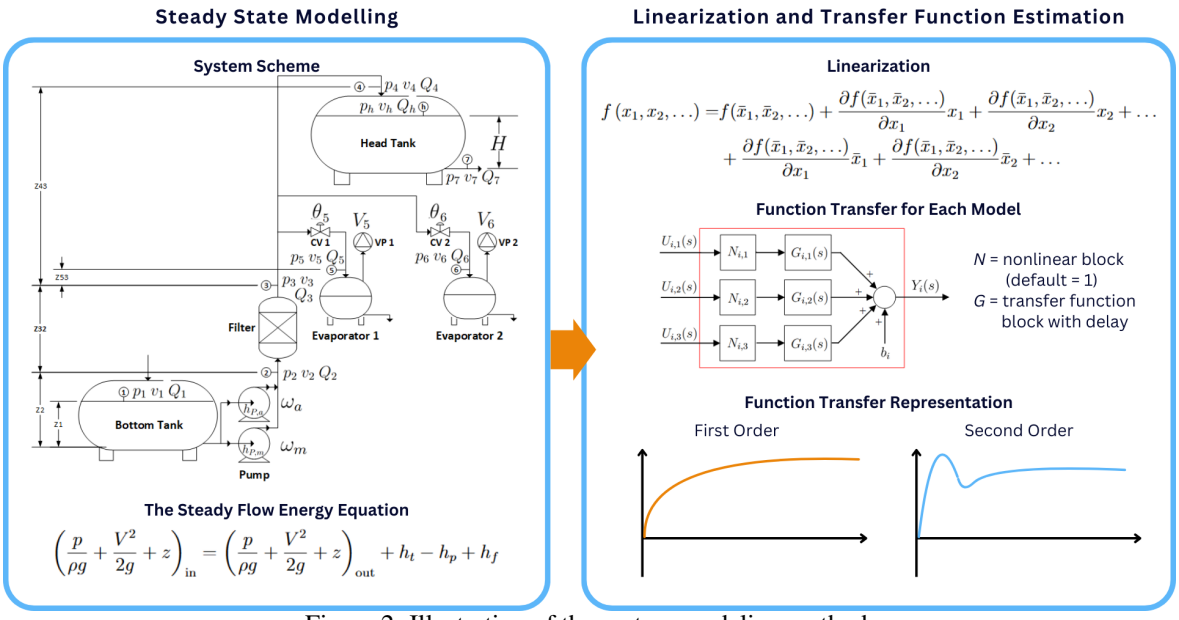

Figure 2. Illustration of the system modeling method.

pump, filter, head tank flow (HTF), head tank level (HTL), evaporator 1 (EVAP 1), and evaporator 2 (EVAP 2), which is used to derive the overall process dynamics using concepts from fluid dynamics. After the static model is derived, it is then linearized at an equilibrium operating condition, which results in a linear transfer function model describing small variation on input-output relationship of each component. Subsequently, the static model of the components is represented as a dynamic model by converting the static gain ratio between variables into transfer functions. These modeling processes are described in the following subsections.

2.1. Pump Model

The pump model is derived by considering inspection points ① and ② in Figure 2. By direct inspection of these points, it can be inferred that the `AUTO` mode (PAM) and the `MANUAL` mode (PMM) of the pump are configured in parallel. Therefore, the value of the total pump head (h_P) can be considered equal to the value of the pump head in the PAM ($h_{P,a}$) and PMM ($h_{P,m}$) modes. Consequently, the total flow rate (Q) of the pump is equal to the sum of the flow rates of the modes PAM (Q_a) and PMM (Q_m), i.e. (1) and (2),

$$h_P = h_{P,a} = h_{P,m} \quad (1) \qquad\qquad Q = Q_a + Q_m. \quad (2)$$

In (1), the value of h_P can be approximated using a polynomial function of the flow rate and pump head variables as follows [10]

$$h_P = \beta_1\omega^2 - \beta_2\omega Q - \beta_3 Q^2. \quad (3)$$

in which β_1, β_2, and β_3 are constant parameters to be estimated. Furthermore, the rotational speeds in the PAM (ω_a) and PMM (ω_m) modes are assumed to be equal such that the flow rate of the PAM mode is the same as that of the PMM mode ($Q_a = Q_m = \frac{1}{2}Q$). Using (1) and (3), the pump head equation can be written as in (4).

$$\begin{aligned} h_P &= \frac{h_{P,a}}{2} + \frac{h_{P,m}}{2} \\ h_P &= \frac{\beta_1{\omega_a}^2 - \beta_2\omega_a Q_a - \beta_3{Q_a}^2}{2} + \frac{\beta_1{\omega_m}^2 - \beta_2\omega_m Q_m - \beta_3{Q_m}^2}{2} \\ h_P &= \frac{1}{2}\beta_1({\omega_a}^2 + {\omega_m}^2) - \frac{1}{4}\beta_2 Q(\omega_a + \omega_m) - \frac{1}{8}\beta_3 Q^2. \end{aligned} \quad (4)$$

Next, the pressure of the bottom tank that is connected to the pump is assumed constant ($\bar{p}_1$) as it is also exposed to atmospheric pressure. Moreover, the velocity of the fluid in the bottom tank and, consequently,

the change of liquid level are assumed to be negligible ($v_1 \approx 0$) due to the large size of the tank. Using the assumption of steady flow conditions [4], the pump head equation can be derived as follows.

$$\begin{aligned}
\frac{\bar{p}_1}{\rho g} + \cancelto{0}{\frac{v_1^2}{2g}} + z_1 =& \frac{p_2}{\rho g} + \frac{{v_2}^2}{2g} + z_2 - h_P + h_{f2} \\
h_P =& \frac{p_2}{\rho g} + \underbrace{\left(\frac{1}{2g{A_2}^2} + k_{f,2}\right)}_{k_2} Q^2 + \bar{z}_{21} + \frac{\bar{p}_1}{\rho g} \\
h_P =& \frac{p_2}{\rho g} + k_2 Q^2 + \bar{z}_{21} + \frac{\bar{p}_1}{\rho g},
\end{aligned} \tag{5}$$

where $\bar{z}_{21}$ is the difference of elevation between inspection points ① and ②, and the coefficient k_2 denotes the total flow rate. Based on (4) and (5), the static pump model (f_1) is obtained as shown in (6).

$$\begin{aligned}
\frac{1}{2}\beta_1({\omega_a}^2 + {\omega_m}^2) - \frac{1}{4}\beta_2 Q(\omega_a + \omega_m) - \frac{1}{8}\beta_3 Q^2 =& \frac{p_2}{\rho g} + k_2 Q^2 + \bar{z}_{21} + \frac{\bar{p}_1}{\rho g} \\
0 =& \frac{p_2}{\rho g} - \frac{1}{2}\beta_1({\omega_a}^2 + {\omega_m}^2) + \frac{1}{4}\beta_2 Q(\omega_a + \omega_m) + \left(\frac{1}{8}\beta_3 + k_2\right) Q^2 + \bar{z}_{21} + \frac{\bar{p}_1}{\rho g} \\
f_1(p_2, \omega_a, \omega_m, Q) \equiv& \frac{p_2}{\rho g} - \frac{1}{2}\beta_1({\omega_a}^2 + {\omega_m}^2) + \frac{1}{4}\beta_2 Q(\omega_a + \omega_m) + \left(\frac{1}{8}\beta_3 + k_2\right) Q^2 + \bar{z}_{21} + \frac{\bar{p}_1}{\rho g}.
\end{aligned} \tag{6}$$

By implementing the multivariabel linearization [6] technique on (6), the linearization $\hat{f}_1$ of the pump model f_1 at the equilibrium $\left(\bar{x}_1 = [\bar{p}_2, \bar{\omega}_a, \bar{\omega}_m, \bar{Q}]\right)$ can be obtained as in (7)

$$\hat{f}_1(p_2, \omega_a, \omega_m, Q) = c_1 p_2 - c_2 \omega_a - c_3 \omega_m + c_4 Q - b_1, \tag{7}$$

where $c_1 = \frac{1}{\rho g}$, $c_2 = \beta_1 \bar{\omega}_a + \frac{1}{4}\beta_2 \bar{Q}$, $c_3 = \beta_1 \bar{\omega}_m + \frac{1}{4}\beta_2 \bar{Q}$, and $c_4 = \frac{1}{4}\beta_2(\bar{\omega}_a + \bar{\omega}_m) + 2\left(\frac{1}{8}\beta_3 + k_2\right)\bar{Q}$, and $b_1 = c_1\bar{p}_2 - c_2\bar{\omega}_a - c_3\bar{\omega}_m + c_4\bar{Q}$. Based on (7), the pump dynamics can be represented as a linear time-invariant system with second-order transfer function with time delay model whose output p_2 is given as in (8):

$$p_2(s) = G_{1,1}(s)\omega_a(s) + G_{1,2}(s)\omega_m(s) - G_{1,3}(s)Q(s) + b_1, \tag{8}$$

Note: what are the values of $G_{i,j}$ in (8)??

2.2. Filter Model

The derivation of the filter model is carried out by considering inspection points ② and ③ in Figure 2. By the inspection of these points, the inlet velocity of the filter (v_2) is assumed to be equal to the outlet velocity of the filter (v_3), thus canceling each other out. From the steady flow equation [4], the static filter model (f_2) is obtained, as shown in (9).

$$\begin{aligned}
\frac{p_2}{\rho g} + \cancelto{0}{\frac{v_2^2}{2g}} + z_2 =& \frac{p_3}{\rho g} + \cancelto{0}{\frac{v_3^2}{2g}} + z_3 + h_{f3} \\
0 =& -\frac{p_2}{\rho g} + \frac{p_3}{\rho g} + k_{f,3} Q^2 + \bar{z}_{32} \\
f_2(p_2, p_3, Q) \equiv& -\frac{p_2}{\rho g} + \frac{p_3}{\rho g} + k_{f,3} Q^2 + \bar{z}_{32},
\end{aligned} \tag{9}$$

where $\bar{z}_{32}$ represents the elevation difference between inspection points ② and ③. Based on the steady flow equation [4] and (9), f_2 is linearized at the equilibrium point of the filter model $\left(\bar{x}_2 = [\bar{p}_2, \bar{p}_3, \bar{Q}]\right)$, resulting in the linearized form $\hat{f}_2$, as shown in (10).

$$\hat{f}_2(p_2, p_3, Q) = -c_5 p_2 + c_6 p_3 + c_7 Q + b_2, \tag{10}$$

where $c_5 = \dfrac{1}{\rho g}$, $c_6 = \dfrac{1}{\rho g}$, $c_7 = 2k_{f,3}\bar{Q}$, and $b_2 = -c_5\bar{p}_2 + c_6\bar{p}_3 + c_7\bar{Q}$. Based on (10), the dynamic filter model is represented as a second-order transfer function with a time delay and output p_3, as shown in (11)

$$p_3(s) = G_{2,1}(s)p_2(s) - G_{2,2}(s)Q(s) + b_2. \tag{11}$$

2.3. Head Tank Flow Model

Based on inspection points ③ to ⑥ and paralel flow system [4], the flow rate at inspection point ③ is equal to the sum of the flow rates at inspection points ④ to ⑥, as shown in (12)

$$Q_3 = Q = Q_4 + Q_5 + Q_6 \tag{12}$$

Based on inspection points ③ and ④, the head tank pressure is known to be constant ($\bar{p}_4$) because it is connected to atmospheric pressure, and the outlet velocity of the filter (v_3) is assumed to be equal to the inlet velocity of the head tank (v_4), thereby canceling each other out. From the steady flow equation [4], the static model of the head tank flow (f_3) is obtained as shown in (13)

$$\begin{aligned}
\frac{p_3}{\rho g} + \cancelto{0}{\frac{v_3^2}{2g}} + z_3 &= \frac{\bar{p}_4}{\rho g} + \cancelto{0}{\frac{v_4^2}{2g}} + z_4 + h_{f4} \\
0 &= -\frac{p_3}{\rho g} + k_{f,4}{Q_4}^2 + \bar{z}_{43} + \frac{\bar{p}_4}{\rho g} \\
f_3(p_3, Q_4) &\equiv -\frac{p_3}{\rho g} + k_{f,4}{Q_4}^2 + \bar{z}_{43} + \frac{\bar{p}_4}{\rho g},
\end{aligned} \tag{13}$$

where $\bar{z}_{43}$ represents the elevation difference between inspection points ③ and ④. From the steady flow equation [4] and (13), f_3 is linearized at the equilibrium point of the head tank flow model $\left(\bar{x}_3 = [\bar{p}_3, \bar{Q}_4]\right)$, resulting in $\hat{f}_3$ as shown in (14)

$$\hat{f}_3(p_3, Q_4) = -c_8p_3 + c_9Q_4 + b_3, \tag{14}$$

where $c_8 = \dfrac{1}{\rho g}$, $c_9 = 2k_{f,4}\bar{Q}$, and $b_3 = -c_8\bar{p}_3 + c_9\bar{Q}_4$. From (14), the dynamics of the head tank flow model are represented as a second-order transfer function with delay, where the output is Q_4, as shown in (15)

$$Q_4(s) = G_{3,1}(s)p_3(s) + b_3. \tag{15}$$

2.4. Head Tank Level Model

Based on inspection points ④, ⓗ, and ⑦ and the law of conservation of mass [4], the change in mass in the head tank ($\dot{m}_h$) is influenced by the mass entering the head tank ($\dot{m}_4$) minus the mass exiting the head tank ($\dot{m}_7$), as shown in (16).

$$\begin{aligned}
\frac{dm}{dt} &= \dot{m}_4 - \dot{m}_7 \\
\rho A_h \frac{dH}{dt} &= \rho(Q_4 - Q_7) \\
H(s) &= \frac{Q_4(s) - Q_7(s)}{A_h s}
\end{aligned} \tag{16}$$

Based on inspection points ⓗ and ⑦, the inlet pressure of the head tank is assumed to be equal to the outlet pressure of the head tank, effectively canceling each other out; the velocity in the head tank (v_h) is negligible due to the large tank area, making the velocity's contribution to height changes insignificant. From the steady flow equation [4], the static model for the head tank level (f_4) is derived, as shown in (17).

$$\begin{aligned}
\cancelto{0}{\frac{p_h}{\rho g}} + \cancelto{0}{\frac{v_h^2}{2g}} + z_h &= \cancelto{0}{\frac{p_7}{\rho g}} + \frac{{v_7}^2}{2g} + z_7 - h_P + h_{f7} \\
0 &= -H + \left(\frac{1}{2g{A_7}^2} + k_{f,7}\right){Q_7}^2 \\
f_4(H, Q_7) &\equiv -H + k_7{Q_7}^2,
\end{aligned} \tag{17}$$

where H represents the liquid level in the head tank, and k_7 is a substitution coefficient for the total flow rate. From the steady flow equation [4] and (17), f_4 is linearized around the equilibrium point of the head tank level model $\left(\bar{x}_4 = [\bar{H}, \bar{Q}_7]\right)$, resulting in the linearized model $\hat{f}_4$ shown in (18).

$$\hat{f}_4(H, Q_7) = -\, c_{10}H + c_{11}Q_7 + b_f, \tag{18}$$

where $c_{10} = 1$, $c_{11} = 2k_7\bar{Q}_7$, and $b_f = -c_{10}\bar{H} + c_{11}\bar{Q}_7$ From (18), the dynamic head tank level model is represented as a transfer function with output Q_7, as shown in (19)

$$Q_7(s) = G_h(s)H(s) + b_4. \tag{19}$$

Equations (16) and (19) can be reduced using block diagram reduction, as shown in Figure 3. The negative feedback of $\frac{1}{A_h s}$ with $G_h(s)$ is represented as $G_{4,1}(s)$, and b_4 is assumed to equal $b_f G_h(s)$ since, under steady-state conditions, $b_f G_h(s)$ resembles a constant. The reduced dynamic model of the head tank level is shown in (20).

Figure 3. Simplification of the head tank level model.

$$\begin{aligned} H(s) =& (Q_4(s) + b_f)\text{feedback}\left\{\frac{1}{A_h s}, G_h(s)\right\} \\ H(s) =& (Q_4(s) + b_f)G_{4,1}(s) \\ H(s) =& G_{4,1}(s)Q_4(s) + b_4 \end{aligned} \tag{20}$$

2.5. Evaporator Model

Based on inspection points ③ and ⑤, the control valve function is assumed to be linear $\left(F_{(\theta_5)} = \frac{1}{\theta_5}\right)$, where θ_5 is the control valve position. The pressure of evaporator 1 (p_5) is influenced by the status of the vacuum pump (V_5) with a negative correlation ($p_5 = -\alpha V_5$), where α is the vacuum pump coeficient. The friction head in the pipeline is neglected ($k_{f,5} = 0$), and the outlet velocity of the filter (v_3) is assumed to be equal to the inlet velocity of evaporator 1 (v_5), effectively canceling each other out.

From the steady flow equation [4], the static model of evaporator 1 (f_5) is obtained as shown in (21)

$$\begin{aligned} \frac{p_3}{\rho g} + \cancelto{0}{\frac{v_3^2}{2g}} + z_3 =& \frac{p_5}{\rho g} + \cancelto{0}{\frac{v_5^2}{2g}} + z_5 + h_{f5} \\ 0 =& -\frac{p_3}{\rho g} - \alpha\frac{V_5}{\rho g} + (k_{f,5} + F_{(\theta_5)}){Q_5}^2 + \bar{z}_{53} \\ f_5(p_3, \theta_5, Q_5) =& -\frac{p_3}{\rho g} - \alpha\frac{V_5}{\rho g} + \frac{1}{\theta_5}{Q_5}^2 + \bar{z}_{53}, \end{aligned} \tag{21}$$

where $\bar{z}_{t3}$ represents the elevation difference between inspection points ③ and ⑤. From the steady flow equation [4] and (21), f_5 is linearized at the equilibrium point of the evaporator 1 model $\left(\bar{x}_5 = [\bar{p}_3, \bar{V}_5, \bar{L}_5, \bar{Q}_5\right)$ into $\hat{f}_5$ as shown in (22)

$$\hat{f}_5(p_3, \theta_5, Q_5) = -\, c_{12}p_3 - c_{13}V_5 + c_{14}\theta_5 + c_{15}Q_5 + b_5, \tag{22}$$

where $c_{12} = \frac{1}{\rho g}$, $c_{13} = \alpha\frac{1}{\rho g}$, $c_{14} = \frac{1}{\bar{\theta}_5^2}\bar{Q}_5^2$, $c_{15} = 2\frac{1}{\bar{\theta}_5}\bar{Q}_5$, and $b_5 = -c_{12}\bar{p}_3 - c_{13}\bar{V}_5 + c_{14}\bar{L}_5 + c_{15}\bar{Q}_5$. From (22), the dynamic model of evaporator 1 is represented as a second-order transfer function with a time delay,

with the output Q_5 shown in (23)

$$Q_5(s) = G_{5,1}(s)\theta_5(s) + G_{5,2}(s)V_5(s) + G_{5,3}(s)p_3(s) + b_5. \tag{23}$$

Based on inspection points ③ and ⑥, the dynamic model of evaporator 2 can be derived similarly to the evaporator 1 model. The dynamic model of evaporator 2 is shown in (24)

$$Q_6(s) = G_{6,1}(s)\theta_6(s) + G_{6,2}(s)V_6(s) + G_{6,3}(s)p_3(s) + b_6. \tag{24}$$

The flow rate characteristics of butterfly-type control valves are nonlinear. Therefore, a nonlinear block is added to the inputs θ_5 and θ_6 with the value $N = 0.312{U_1}^2 - 3.7402U_1$, obtained from the quadratic regression of historical process data.

2.6. System Model Representation

The system model representation shown in Figure 4 is derived from combining the component dynamic models in (8), (11), (15), (20), (23), and (24). There are three inputs in `AUTO` mode: pump in `AUTO` mode (PAM) rotational speed (ω_a), control valve 1 position (θ_5), and control valve 2 position (θ_6). There are also three inputs in `MANUAL` mode: pump in `MANUAL` mode (PMM) rotational speed (ω_m), status of vacuum pump 1 (V_5), and status of vacuum pump 2 (V_6). The output of the system is the solution height in the head tank (H), where the inlet flow rates of evaporator 1 (Q_5) and evaporator 2 (Q_6) are not the primary focus of the control system.

As seen in Figure 4, a decrease in the inlet flow rate to the evaporator causes an increase in pressures p_2 and p_3, which consequently increases the inlet flow rate to the head tank (Q_4) and gradually affects the solution height in the head tank. Therefore, DCS operators often reduce the rotational speed of the pump in `MANUAL` mode to compensate for the increased inlet flow rate to the evaporator, aiming to maintain a more consistent solution height in the head tank.

3. CONTROL SYSTEM DESIGN

In the spinbath circulation system, the solution height setpoint in the head tank is set at 96%, with the criterion that the deviation from the head tank solution height must not exceed 1%. This aims to maintain the flow consistency in the spinning machine and prevent leakage. However, changes in the evaporator flow rate can impact the solution height in the head tank, and the evaporators need to be stopped and restarted for cleaning processes. Therefore, based on the system model representation shown in Figure 4, three control system configurations are designed to maintain the solution height in the head tank: (i) single-loop (SL), (ii) conventional cascade (CC), and (iii) summed-setpoint cascade (SSC).

3.1. Single-Loop Configuration

In the single-loop (SL) control system configuration shown in Figure 5, the solution height in the head tank is controlled by a single feedback controller (C_1), with R as the solution height setpoint in the head tank. The head tank solution height controller manipulates the rotational speed of the PAM and gradually affects the solution height in the head tank. In this configuration, if there is a change in the evaporator flow rate setpoint, the head tank solution height controller only responds after a change in the head tank solution height occurs, resulting in a slow response and significant deviation. There are two additional feedback controllers (C_6 and C_7) to control the evaporator 1 and evaporator 2 flow rates, with their respective setpoints being D_1 and D_2.

3.2. Conventional Cascade Configuration

To address the limitations of the single-loop control system configuration, a conventional cascade (CC) control system configuration, as shown in Figure 6, is proposed. In this configuration, the outer-loop controller (C_2) controls the head tank solution height (H) using R as the setpoint, while the inner-loop controller (C_3) controls the inlet flow rate to the head tank (Q_4) by manipulating the PAM rotational speed. However, similar to the single-loop configuration, changes in the evaporator flow rate setpoint are not directly compensated, although the response to flow rate deviation is faster.

3.3. Summed-Setpoint Cascade Configuration

Therefore, the summed-setpoint cascade (SSC) configuration is designed to address the issues in the previous two configurations, as shown in Figure 7. In this configuration, the outer-loop controller (C_4) controls the head tank solution height (H) with R as its setpoint, while the inner-loop controller (C_5) controls the total flow rate $\big(Q_4 + K_c(Q_5 + Q_6)\big)$, where K_c is the coupling constant. As a result, changes in the evaporator flow rate setpoint are directly compensated, allowing the controller to manipulate the PAM rotational speed before any deviation occurs.

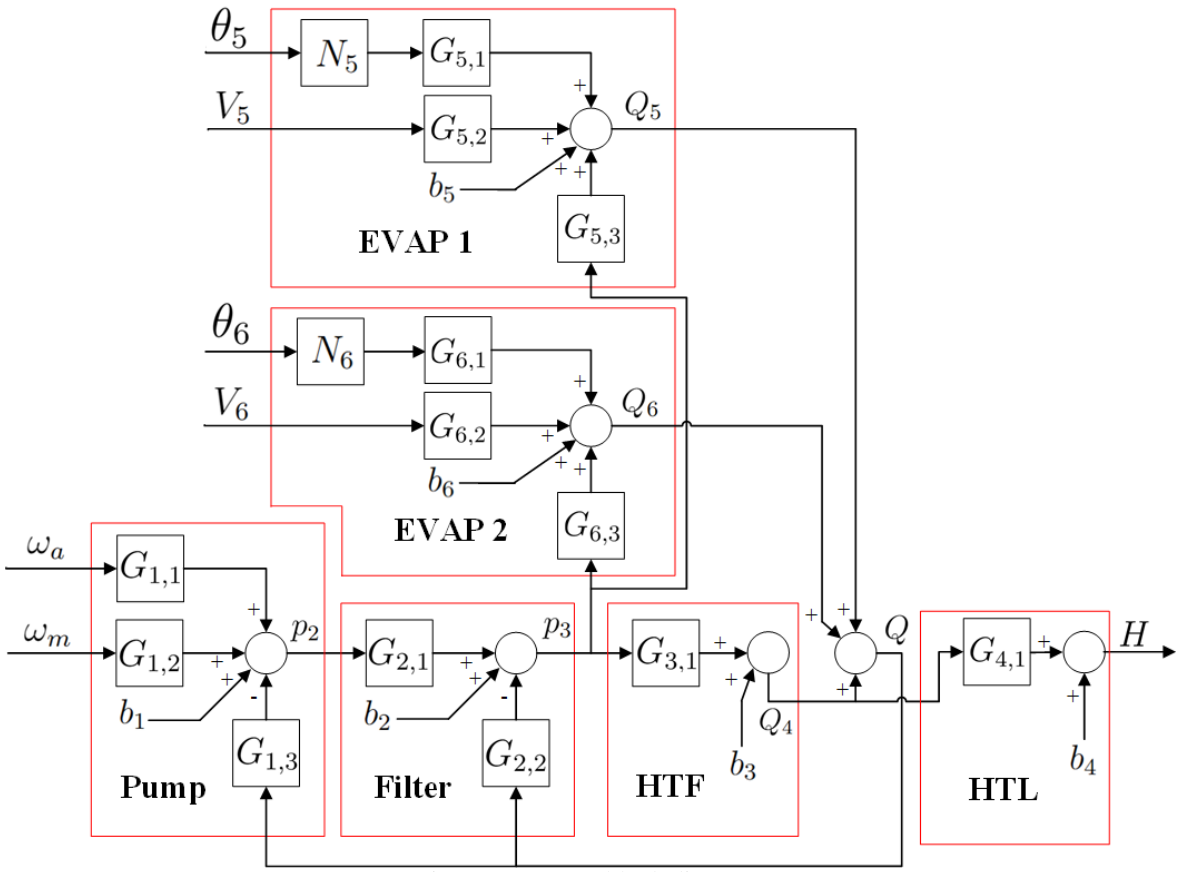

Figure 4. System block diagram.

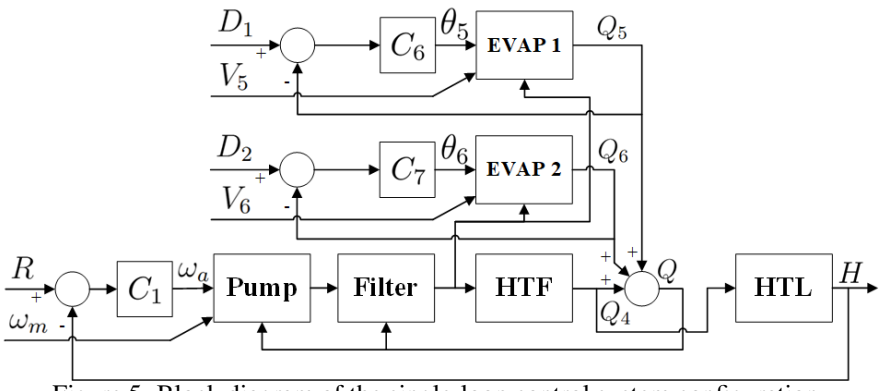

Figure 5. Block diagram of the single-loop control system configuration.

3.4. Control System Demonstration

The demonstration of the control system aims to validate the proposed concept on a simplified model to verify the effectiveness of the control system design. At this stage, the manual mode input (V_5, V_6, ω_m) and the base gain (b_1, b_2, b_3, b_4, b_5, b_6) in the system are neglected for simplification purposes. The dynamics of the components are modeled as first-order systems, with the parameters adjusted according to the characteristics of each component, estimated from data, as shown in Table 1. The PID controller parameters are tuned based on system criteria, as shown in Table 2, with a coupling constant (K_c) value of 1.

The step response simulation for D_1 was performed on all three control system configurations to evaluate the system's performance in maintaining the liquid level in the head tank against changes in evaporator flow rate setpoints. This simulation assumes zero initial conditions with a simulation time of 70 seconds. The step response plot for D_1 is shown in Figure 8, and the resulting characteristics, along with the Integral Absolute Error (IAE) values, are presented in Table 3. The IAE indicates the area under the curve relative to the reference line (zero), where the summed-setpoint cascade configuration has the smallest value. It is evident that

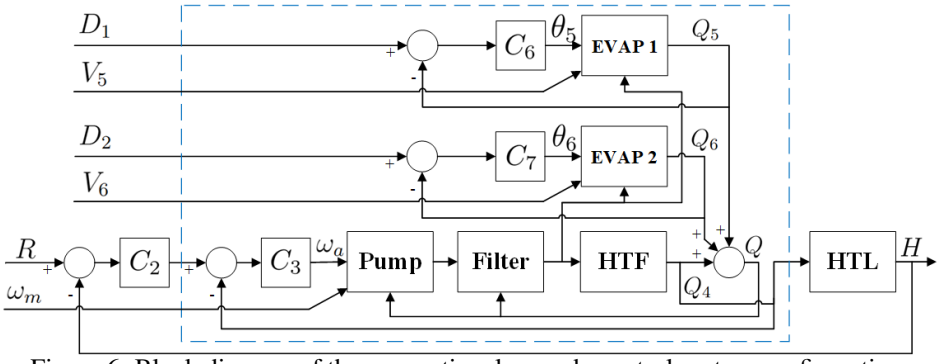

Figure 6. Block diagram of the conventional cascade control system configuration.

Table 1. Simplified component dynamic model parameters.

i	Pump		Filter		HTF	HTL	Evap 1		Evap 2	
j	1	3	1	2	1	1	1	3	1	3
K_s	1	0.2	1	0.2	1	1	1	1	1	1
τ	1	1	1	1	1	10	3	3	3	3

Table 2. Simplified system PID parameters.

Controller	System Criteria		PID Parameters		
	Response Time	Transient Behavior	K_p	K_i	K_d
C_1	20s	0.7	1.2277	0.1565	0
C_2 & C_4	8s	0.7	0.9687	0.0971	0
C_3 & C_5	20s	0.7	0.3224	0.3519	0
C_6 & C_7	3s	0.7	1.2321	1.2440	0

Table 3. Step response characteristics of D_1.

Information	SL	CC	SSC
Max value	0.001	0.036	0.015
Min value	-0.127	-0.074	-0.024
Peak error	0.127	0.074	0.024
IAE	2.599	1.153	0.443

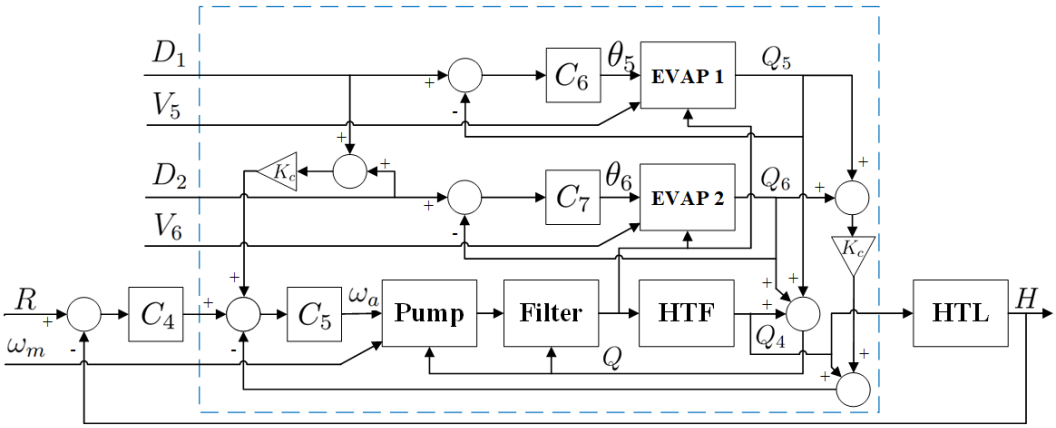

Figure 7. Block diagram of the summed-setpoint cascade control system configuration.

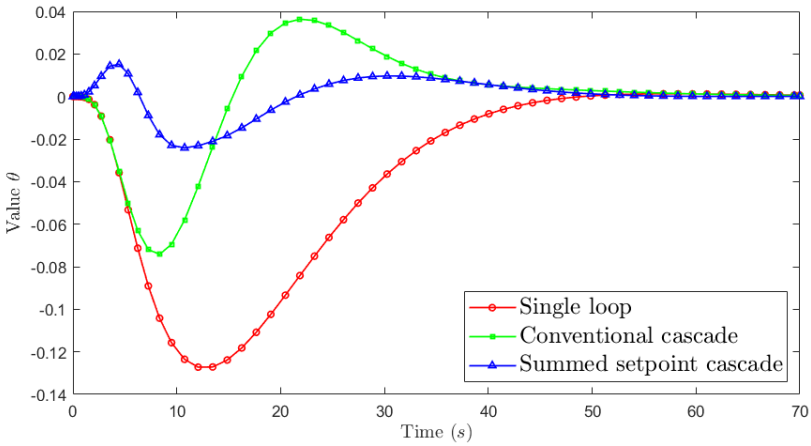

Figure 8. Step response plot for D_1.

the summed-setpoint cascade configuration exhibits smaller peak error and IAE compared to the single-loop configuration, thus enhances the robustness of the spinbath circulation system on the simplified model.

4. SYSTEM IDENTIFICATION

The system identification method, illustrated in Figure 9, begins with data collection from the system by recording historical data, which includes process and manipulation variables under steady-state conditions with several disturbances. The collected data is then processed to handle missing data using linear interpolation and estimation to approximate variables without sensors. After processing the data using Microsoft Excel, curve fitting and optimization are performed on the component dynamic model as a second-order system with a time delay. The output of each component dynamic model ($Y_{i,est}$) is represented in the general form (25), and the transfer function for each input ($G_{i,j}$) is represented in the general form (26)

$$Y_{i,est} = b_i + \sum_{j=1}^{m} N_{i,j} G_{i,j} U_{i,j} \tag{25}$$

$$G_{i,j} = \frac{K_{s,i,j}\omega_{n,i,j}{}^2 e^{-t_{\mathrm{d},i,j}s}}{s^2 + 2\zeta_{i,j}\omega_{n,i,j}s + \omega_{n,i,j}{}^2}, \tag{26}$$

where $i = 1, 2, \ldots, 6$ indicates the component index, and $j = 1, 2, \ldots$ indicates the input index.

The *curve fitting* process aims to adjust the model parameters, such as steady-state gain (K_s), natural frequency (ω_n), damping ratio (ζ), and time delay (t_d), so that the component dynamic model output ($Y_{i,est}$) closely resembles the actual data ($Y_{i,act}$). The manually fitted parameters serve as initial guesses for the optimization method, maximizing the fit between the model estimation and the actual data, as shown in (27).

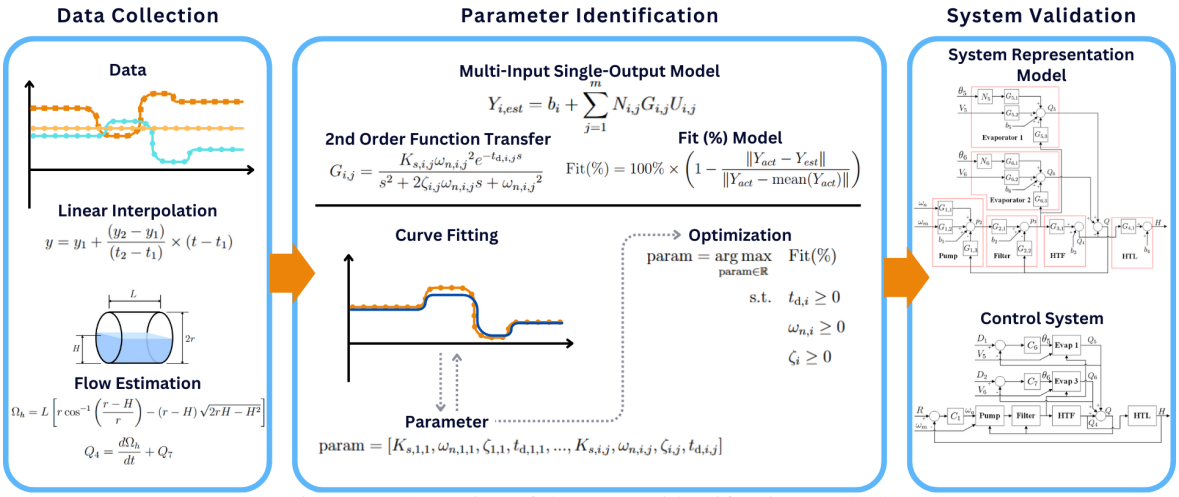

Figure 9. Illustration of the system identification method.

$$\text{Fit}(\%) = 100\% \times \left(1 - \frac{\|Y_{act} - Y_{est}\|}{\|Y_{act} - \text{mean}(Y_{act})\|}\right), \tag{27}$$

where $\|.\|$ denotes the *Euclidean Norm* $\left(\|x\| = \sqrt{x_1{}^2 + x_2{}^2 + \ldots}\right)$. This degree of agreement indicates how well the model represents the actual system behavior. The model optimization is conducted numerically by solving the problem in (28).

$$\begin{aligned} \text{param} = \arg\max_{\text{param}\in\mathbb{R}} \quad & \text{Fit}(\%) \\ \text{s.t.} \quad & t_{\text{d},i} \geq 0 \\ & \omega_{n,i} \geq 0 \\ & \zeta_i \geq 0 \end{aligned} \tag{28}$$

The optimization method used is the Nelder-Mead simplex method [11]. Finally, the system model representation using a single-loop control configuration is compared with the actual data and validated through R^2 equation shown as (29)

$$R^2(\%) = 100\% \times \left(1 - \frac{\sum\left(Y_{act} - Y_{est}\right)^2}{\sum\left(Y_{act} - \text{mean}(Y_{act})\right)^2}\right). \tag{29}$$

The system identification analysis is divided into two subsections, namely the dynamics model of components and the system model representation.

4.1. Dynamics Model of Components

System identification is performed on the dynamics model of components derived from system modeling in subsection 2., based on steady-state data with deviations according to the method discussed in subsection 4.. The comparison of the estimated dynamics model of components (blue) with actual data (red), including all inputs (black), is shown in Figures 10. According to Table 4, which presents parameters and fit values, the polarity of the static gain constant (K_s) for each component is consistent with the system modeling polarity in subsection 2..

The obtained fit values vary depending on the complexity and response deviation of each component. For instance, the fit values for the pump model and evaporator 1 model indicate high conformity, at 80.16% and 89.24%, respectively, suggesting that the model accurately represents their dynamics. However, the HTF model has a low fit value (23.93%) due to small data deviations, where estimation errors significantly impact the fit value. From Figure 10, it can be seen that the model captures the fluctuations present in the actual data. Overall, this model provides a solid foundation for analyzing and reconstructing the system model representation.

Table 4. Parameters of the component dynamics model.

i	j	Parameter					$R^2(\%)$
		K_s	ω_n	ζ	t_d	b	
Pump	1	0.0344	1.3656	1.0704	0.0064	-0.7229	96.06
	2	0.0367	1.8317	1.0489	0.0532		
	3	-0.0002	2.1555	1.6498	0.0163		
Filter	1	0.6448	1.2536	1.8485	0.0000	0.2797	95.34
	2	-0.0001	0.9484	1.4388	0.0001		
HTF	1	1317.0000	1.6000	0.7000	0.1000	-1569.9000	42.14
HTL	1	0.0358	0.0490	1.7484	0.0000	3.0457	71.60
EVAP 1	1	0.0277	0.1940	0.4237	0.0020	-53.7957	98.84
	2	24.6493	0.0042	0.8878	0.0002		
	3	24.6052	8.0000	0.4210	0.0013		
EVAP 2	1	0.0265	0.1913	0.4001	0.0138	-41.5136	97.34
	2	20.1535	0.0052	0.9331	0.0011		
	3	26.1523	6.1351	0.3515	0.0010		

4.2. System Model Representation

The comparison of the system model representation estimation using a single-loop control configuration in Figure 5 with process data during the shutdown and activation of the evaporator is performed using Simulink to validate the system identification. The PID parameters for each controller are determined based on the data collection values. For controller C_1, the parameters used are $K_p = 0.0001$, $K_i = 0.0060$, and $K_d = 0$; whereas for controllers C_6 and C_7, the parameters used are $K_p = 0.0085$, $K_i = 0.0016$, and $K_d = 0$. The comparison of the estimated system model representation using a single-loop control configuration (red) with actual data (blue) is shown in Figure 11. The obtained fit value is 86.7382%, with a R^2 fit model. Additionally, the data contains severe noise, which worsens the fit value of the model. This indicates that the system model representation can represent the actual dynamics of the spinbath circulation system with control.

5. SIMULATION

The simulation of evaporator shutdown and activation is conducted to analyze the capability of the three control system configurations in maintaining the liquid level in the head tank at its setpoint of 96% with

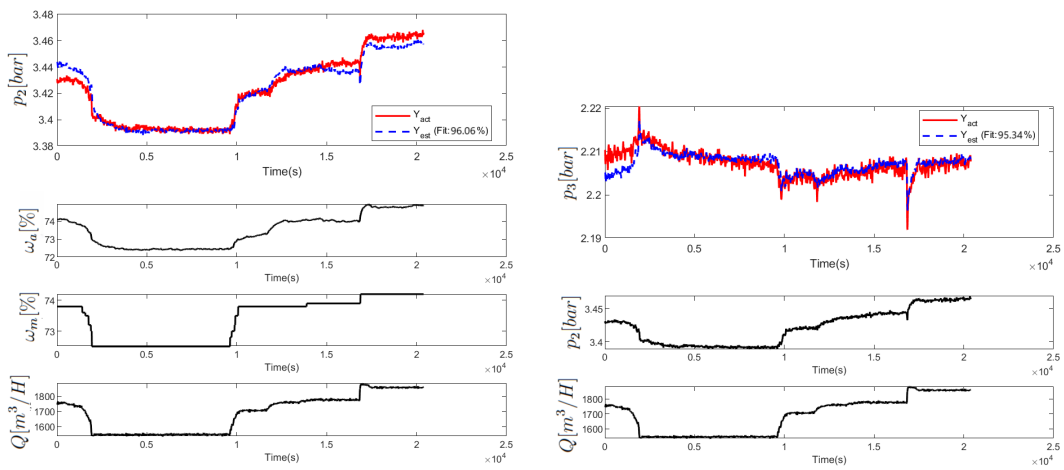

(a) Pump (b) Filter

Figure 10. Comparison of component dynamics model estimation with actual data.

a tolerance of $\pm 1\%$. The control system simulations for the single-loop, conventional cascade, and summed-setpoint cascade configurations, as shown in Figures 5, 6, and 7, are carried out using Simulink. The tuned controller parameters are presented in Table 5, with a gain value of $K_c = 0.45$. In the simulation of the evaporator shutdown and activation process, the system's input and setpoint are modified to resemble actual process conditions. The setpoint of the evaporator flow rate and the vacuum pump condition are changed from their steady-state values to zero and then back to their steady-state values within 10,000 seconds.

There are two simulation modes, which is (i) Semi-automatic mode, where the manual pump speed (ω_m) is adjusted to reduce deviations, and (ii) Automatic mode, where the manual pump speed remains unchanged. The simulation characteristics are shown in Table 6, and the output-setpoint-input graph of the simulation is presented in Figure 12, with dashed lines indicating the boundary between the semi-automatic mode (left) and the automatic mode (right). The peak error represents the maximum deviation of the liquid level in the head tank from the setpoint of 96%, and the integral absolute error (IAE) indicates the area of the graph outside the setpoint line. The following is a discussion for each simulation mode:

5.1. Semi-Automatic Mode

In the semi-automatic mode, it is observed that the single-loop configuration has the highest peak error and IAE values, with values of 0.4066 and 34.9133, respectively. The conventional cascade configuration has the smallest IAE, which is 44% smaller compared to the single-loop configuration. The peak error in the conventional cascade configuration is 6.15% larger compared to the summed-setpoint cascade configuration. The summed-setpoint cascade configuration has the smallest peak error, which is 24.47% smaller compared to the single-loop configuration. The IAE of the summed-setpoint cascade configuration is 19.34% larger compared to the conventional cascade configuration.

5.2. Automatic Mode

In the automatic mode, it is observed that the single-loop configuration has the highest peak error and IAE values, with values of 0.7501 and 64.8151, respectively. The conventional cascade configuration has an IAE 20.33% larger compared to the summed-setpoint cascade configuration. The peak error in the conventional cascade configuration is 6.15% larger compared to the summed-setpoint cascade configuration.

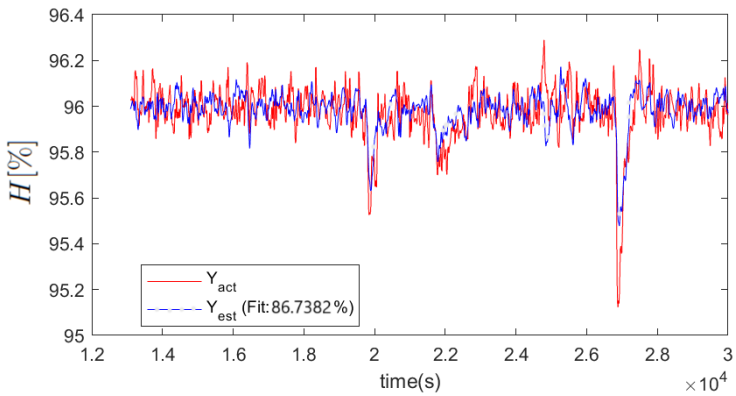

Figure 11. Comparison of the system model representation estimation with actual data.

Table 5. Controller Parameters.

Controller	System Criterion		PID Parameter		
	Waktu Respons	Perilaku Transien	K_p	K_i	K_d
C_1	100s	0.7	1.4351	0.02917	0
C_2 & C_4	40s	0.7	0.0001	0.0022	0
C_3 & C_5	100s	0.7	42.994	0.6522	514.6444
C_6 & C_7	15s	0.7	0.0196	0.00414	0

Table 6. The characteristic of evaporator shutdown and activation.

Information	**SL**		**CC**		**SSC**	
	semi	auto	semi	auto	semi	auto
Max value	96.4066	96.5943	96.2359	96.3091	96.2997	96.2455
Min value	95.6185	95.2499	95.6740	95.6670	95.6929	95.7096
Peak error	0.4066	0.7501	0.3260	0.3330	0.3071	0.2904
IAE	34.9133	64.8151	19.6422	25.0783	23.4416	20.8416

The summed-setpoint cascade configuration has the smallest peak error, which is 61.29% smaller compared to the single-loop configuration. The IAE of the summed-setpoint cascade configuration is the smallest, with a value 67.84% smaller compared to the single-loop configuration.

From the analysis of both semi-automatic and automatic modes, it can be concluded that the single-loop configuration, in both modes, results in the highest peak error. Moreover, the single-loop configuration produces a larger IAE than the other configurations, indicating the most extreme deviation in the liquid level in the head tank. The conventional cascade configuration in semi-automatic mode exhibits the lowest IAE, which is 19.6422, indicating the smallest deviation impact. The summed-setpoint cascade configuration in automatic mode has the smallest peak error, with an IAE that is not significantly different from the conventional cascade configuration in semi-automatic mode, at 20.8416. Based on these results, the summed-setpoint cascade configuration in automatic mode provides the smallest deviation, as seen from both the peak error and IAE values, which are less than 7% greater than the IAE of the conventional cascade configuration in semi-automatic mode.

6. CONCLUSION

The system modeling process begins with deriving the static model of each component based on the designed scheme, followed by linearization and transfer function representation. Missing data is handled using linear interpolation, while the inlet flow rate of the head tank is estimated from the solution level dynamics.

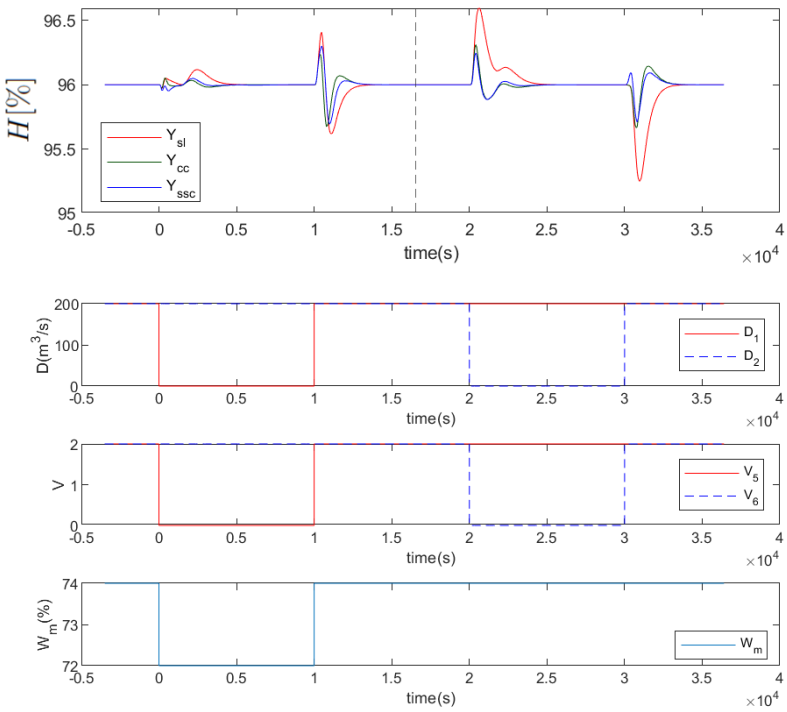

Figure 12. The simulation of evaporator shutdown and activation.

The dynamic model of each component is represented as a second-order system with a time delay, with parameters estimated using curve fitting and optimization, achieving a model fit of 86.7382%. The control system with a summed-setpoint cascade configuration in automatic mode outperforms the single-loop configuration in minimizing solution level deviations in response to evaporator flow setpoint changes.

ACKNOWLEDGEMENT

The acknowledgment section is optional. The funding source of the research can be put here.

REFERENCES

[1] APR, *Asia Pacific Rayon: Process and Technical Description Modules*, Asia Fibre Trading Pte Ltd, Accessed on: 2020.

[2] A. G. Wilkes, "The viscose process," *Regenerated cellulose fibres*, pp. 37–61, 2001.

[3] I. S. Mendes, A. Prates, and D. V. Evtuguin, "Production of rayon fibres from cellulosic pulps: State of the art and current developments," *Carbohydrate Polymers*, vol. 273, p. 118466, 2021.

[4] F. White, *Fluid Mechanics*. McGraw-Hill Education, 2015.

[5] B. Munson, W. Huebsch, T. Okiishi, and A. Rothmayer, *Fluid Mechanics*. Wiley, 2013. [Online]. Available: https://books.google.co.id/books?id=S0aaMQEACAAJ

[6] K. Ogata, *Modern Control Engineering*. Prentice Hall, 2010.

[7] A. Arda Ozdemir and S. Gumussoy, "Transfer function estimation in system identification toolbox via vector fitting," *IFAC-PapersOnLine*, vol. 50, no. 1, pp. 6232–6237, 2017, 20th IFAC World Congress. [Online]. Available: https://www.sciencedirect.com/science/article/pii/S2405896317315045

[8] M. Ferrari and A. Visioli, "An educational interactive software tool to learn cascade control design," *IFAC-PapersOnLine*, vol. 56, no. 2, pp. 7561–7566, 2023.

[9] K. Chandran *et al.*, "Modified cascade controller design for unstable processes with large dead time," *IEEE Access*, vol. 8, pp. 157 022–157 036, 2020.

[10] G. Janevska, "Mathematical modeling of pump system," in *Electronic International Interdisciplinary Conf.*, vol. 2, 09 2013, pp. 455–458.

[11] J. C. Lagarias, J. A. Reeds, M. H. Wright, and P. E. Wright, "Convergence properties of the nelder–mead simplex method in low dimensions," *SIAM Journal on optimization*, vol. 9, no. 1, pp. 112–147, 1998.

BIOGRAPHIES OF AUTHORS

The recommended number of authors is at least 2. One of them as a corresponding author.
Please attach clear photo (3x4 cm) and vita. Example of biographies of authors (9 pt)

Immanuel Raynaldo Santjoko is currently pursuing his B.Eng. degree in electrical engineering at Parahyangan Catholic University, Indonesia. His research interests include robotics, systems identification, and industrial process control systems.

Tua Agustinus Tamba received both MSEE and PhD degrees in electrical engineering from the University of Notre Dame, USA, in 2016, the M.Sc. degree in mechanical engineering from Pusan National University, Republic of Korea, in 2009, and the B.Eng. degree in engineering physics from Institut Teknologi Bandung, Indonesia, in 2006. He is currently an associate professor in the Department of Electrical Engineering at Parahyangan Catholic University, Indonesia. His main research interests include dynamical systems, control theory, and optimization with applications in mechatronics, robotics, automation, and networked dynamical systems.

Ali Sadiyoko